J Appl Electrochem (2013) 43:199–208
DOI 10.1007/s10800-012-0514-1

ORIGINAL PAPER

Growth and photoelectrochemical behaviour of electrodeposited ZnO thin films for solar cells

R. Inguanta · C. Garlisi · T. Spanò · S. Piazza · C. Sunseri

Received: 18 July 2012 / Accepted: 3 December 2012 / Published online: 19 December 2012

Abstract Thin zinc oxide films were deposited potentiostatically from zinc nitrate aqueous solutions on ITO substrates. The influence of experimental parameters (temperature, electrolyte concentration, deposition potential) on structure and morphology of films was investigated. Deposited films were generally polycrystalline in structure, even if growth according to preferential planes occurs in certain conditions. The effect of thermal treatments in air at 150 and 350 °C was also studied. In some cases, Cl species were incorporated into deposit by adding zinc chloride to the electrolyte. A photoelectrochemical investigation, performed in neutral solution before and after thermal treatment, gives more information on film structure and reveals improvement of n-type semiconducting properties after annealing, suggesting diminution of defects and traps originated from the disordered regions of the oxide. In fact, after thermal treatment, the optical gap of the films decreases towards the value reported for the crystalline oxide. No apparent benefits in the semiconducting properties of the films were observed after incorporation of Cl species into the films.

Keywords ZnO · Solar cells · Electrodeposition · Photocurrent

Electronic supplementary material The online version of this article (doi:10.1007/s10800-012-0514-1) contains supplementary material, which is available to authorized users.

R. Inguanta · C. Garlisi · T. Spanò · S. Piazza (✉) · C. Sunseri
Laboratorio Chimica Fisica Applicata, Dipartimento di Ingegneria Chimica Gestionale Informatica Meccanica, Università di Palermo, Viale delle Scienze Bdg. 6, 90128 Palermo, Italy
e-mail: salvatore.piazza@unipa.it

1 Introduction

Current research on solar cells suggests that thin-film cells could be a valid alternative to the traditional silicon-based ones [1]. As an example, solar cells based on $Cu(In,Ga)Se_2$ (CIGS) single-junction display a conversion efficiency of more than 20 % [2]. Hence, effort was devoted to obtain thin-film solar cells through low cost and easily scalable processes [3]. In this context, electrodeposition can play a key role, because it is a very simple and quick technique for obtaining good-quality, large-area films compared to other fabrication methods [4]. Using this technique, we have obtained CIGS nanowires [5] and thin-films on flexible substrate with good success.

However, the same technique can be employed for the fabrication of the entire device, depositing further layers on the absorber material. In this study, we present a detailed study on the electrodeposition of thin ZnO films. This material is considered amongst the most efficient transparent conductive oxide for solar cell applications, due to its structural and optoelectronic properties [6, 7]. In fact, owing to its large band gap, ZnO presents a good transparency in the visible wavelength range [8].

In order to grow ZnO thin films, several fabrication methods have been proposed, like sol–gel [9], ionic layer adsorption and reaction [10], chemical bath deposition [11], spray pyrolysis [12], metal–organic chemical vapour deposition [13], sputtering [14], electroless [15] and electrodeposition [16]. Amongst these methods, electrodeposition is a very simple, low cost and easily scalable technique [17, 18]. Besides, arrays of ZnO nanorods and nanowires can be grown by electrodeposition without using a template [19–21]. These nanostructures grow along their *c*-axis of their hexagonal cell and they have attracted much attention owing to interesting optical and electrical

properties [22]. Recently, electrodeposited ZnO nanowires were converted in highly oriented nanotubes by a simple selective dissolution [23].

Although, low resistive n-type ZnO can be obtained without any external doping, due to the formation of native donors such as oxygen vacancies and interstitial Zn ions [24], external ZnO doping is reported to improve the performance. Typical dopants of ZnO are Al [25], N [26], B [27] and Cl [28]. In this study, we have focused our attention on doping of ZnO with Cl. In particular, the possibility to use electrodeposition for obtaining ZnO:Cl is discussed: in fact Lincot and coworkers [29] have shown that high efficiency (up to 15.8 %) CIGS-based solar cells can be obtained using electrodeposited ZnO:Cl as transparent conducting oxide front contact.

In the following, we report the results concerning a systematic study on the fabrication of ZnO thin films obtained by potentiostatic deposition from different electrolytic baths. The effect of thermal treatments, carried out at different temperatures and for different times, on the properties of the electrodeposited films was also discussed.

2 Experimental

ZnO films were deposited electrochemically on ITO substrates, supported by polyethylene terephthalate (PET) or glass. Before deposition, different substrate pre-treatments were investigated, in order to obtain uniform deposits [30]. For depositions on ITO substrates, a simple ultrasonic degreasing in organic solvents (first step: acetone, second step: isopropilic alcohol; 15 min each step) was often adopted. After this treatment, ITO surface was analysed by scanning electron microscopy (SEM) analysis to exclude its possible swelling or cracking during the ultrasonic treatment. Electrochemical experiments were performed using a PAR potentiostat/galvanostat (PARSTAT, mod. 2273). Depositions were carried out potentiostatically under nitrogen atmosphere in a three-electrode cell having a Pt counter-electrode and a mercury sulphate reference electrode (MSE, $E = +0.65$ V/NHE), from de-aerated aqueous solutions of $Zn(NO_3)_2{\cdot}6H_2O$ with different concentrations (0.01–0.1 M) and at various temperatures (from 40 to 60 °C). The effect of deposition potential in the interval −1.2 to −1.4 V(MSE) was also investigated. When chlorine incorporation into the films was desired, $ZnCl_2$ was added to the electrolyte in different amounts to grow ZnO films with a variable Cl content. During depositions, current versus time curves were monitored and acquired through POWERSUITE software. Active sample area was delimited by means of an insulating lacquer.

Films morphology was analyzed by SEM, using a FEI FEG-ESEM (mod. QUANTA 200) equipped with an energy disperse spectroscopy (EDS) detector. Films were also characterized by XRD analysis, using a ItalStructures (APD2000) diffractometer, both having the Cu Kα radiation ($\lambda = 0.154$ nm) as the source, with a step of 0.02° and a measuring time of 0.5 s for each step, and Raman spectroscopy, using a Renishaw, inVia Raman Microscope, equipped with a He–Ne laser beam having a spot size of 2 μm and calibrated by means of the Raman peak of a polycrystalline Si (520 cm^{-1}). XRD peaks were identified by comparison with the ICDD Database [31].

Photoelectrochemical behaviour of the films was investigated at room temperature in aerated 0.1 M Na_2SO_4 solution (pH 5.6), using a cell having flat quartz windows for allowing sample illumination. A Pt net served as the counter electrode, and the reference was a MSE electrode. Monochromatic irradiation was achieved using a UV–Vis Xenon lamp (Oriel) coupled to a UV–Vis monochromator (Baush & Lomb), mounted in an optical line equipped with quartz optics. For improving photocurrent resolution, a two-phase lock-in amplifier (EG&G, mod. 5206) was used in connection with a mechanical chopper (frequency: 10 Hz). Data were acquired by a desk computer through an analogic interface using a LABVIEW™ 7 software and processed according to home-written programs. Photocurrent spectra reported below are corrected for the photon emission at each wavelength of the lamp/monochromator system; the latter was detected previously using a calibrated thermopile (Newport).

3 Results and discussion

3.1 ZnO electrodeposition

Deposition of ZnO films from aqueous zinc nitrate solutions [32, 33] occurs through the well-known mechanism of base electrogeneration. This foresees reduction of nitrate ions at the negatively biased working electrode:

$$NO_3^- + H_2O + 2e^- \rightarrow NO_2^- + 2OH^- \quad (E = 0.0835 - k\text{pH}) \tag{1}$$

where k is $\log(RT/F)$ ($R = 8.314$ J/mol °K, $F = 96485$ C/mol).

Reaction (1) provokes a sharp increase of local pH al the electrode/electrolyte interface, with subsequent precipitation of more or less hydrated oxide:

$$Zn^{2+} + 2OH^- \Rightarrow Zn(OH) \Leftrightarrow ZnO \downarrow + H_2O \tag{2}$$

We have checked the influence of the experimental parameters (nitrate concentration, deposition potential and temperature) on the kinetics of deposition as well as on film morphology and structure.

Figure 1 shows the current versus time curves during depositions performed at −1.4 V/MSE and different temperatures from the same solution. At 40 °C, only a small current circulates, whilst at 60 °C cathodic c.d. initially increases and then reaches an almost constant value of about −0.4 mA cm^{-2}. The different deposition curves reveal different morphology and structure of the films. A compact ZnO layer, covering uniformly all substrate area exposed to the solution, was obtained at 60 °C, whilst at lower temperature deposit was discontinuous. Moreover, films deposited at 60 °C display a higher crystalline degree, as shown by the XRD patterns of Fig. 2. The diffraction peaks, all matching a polycrystalline zinc oxide phase (ICDD card 36-1451) [31], are sensibly higher and narrower with respect to those of film deposited at lower temperature, where also peaks relative to some crystalline planes are absent. From main peaks of patterns in Fig. 2 a mean crystallite size was calculated applying the Schrerer's equation [34], equal to about 33 nm for the film deposited at 60 °C and ∼15 nm for the oxide deposited at 40 °C.

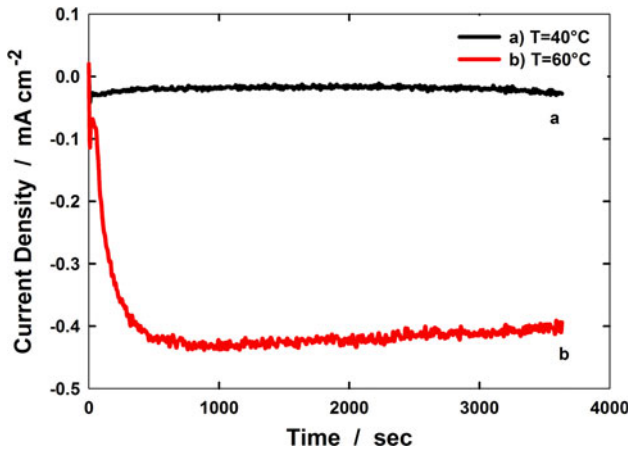

Fig. 1 Current density versus time during potentiostatic deposition of ZnO films from a 0.05 M $Zn(NO_3)_2{\cdot}6H_2O$ solution at −1.4 V(MSE) for different temperatures: *a* 40 °C; *b* 60 °C

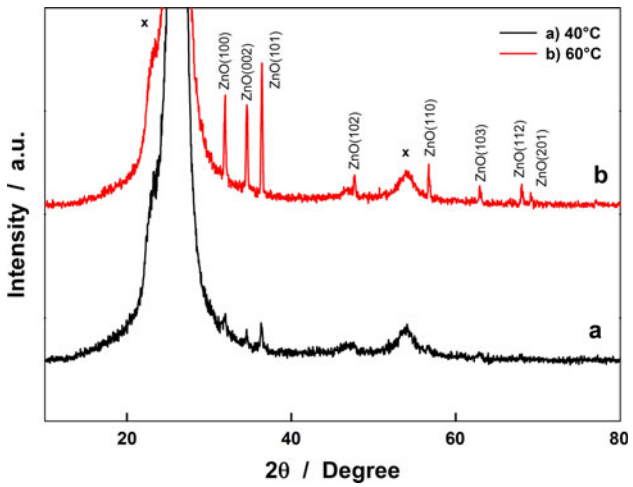

Fig. 2 XRD diffraction patterns for the ZnO films of Fig. 1. *Peaks* marked with *x* are relative to the ITO/PET substrate

As for the film thickness, the analysis of the cross-sectional view of the samples (see Fig. S1 in the electronic supplementary material, ESM) reveals that deposits obtained at 60 °C have a mean value of 700 nm, uniform along the section of oxide. ZnO films obtained at 60 °C were also analyzed by Raman spectroscopy. A typical spectrum is shown in Fig. 3, where also a spectrum of ITO/PET substrate is reported for comparison. Lowering of ITO/PET vibration bands is likely due to screening by the ZnO deposit. Apart from ITO/PET bands, three Raman bands at 331, 410 and 438 cm^{-1} and a weak and broad band at 520–590 cm^{-1} are observed that are characteristic of ZnO [35, 36]. The band at 331 cm^{-1} is a second order Raman scattering, and can be assigned to E_{2H}–E_{2L} mode (multi phonon process). Peak at 410 cm^{-1} is attributed to E_1(TO), whilst the band at 438 is a first ordered Raman scattering attributed to the optical phonon E_{2H} mode of the wurtzite hexagonal phase of ZnO [9]. This mode is asymmetric, probably due to phonon confinement for the presence of nano-crystallites [37, 38] or to the an-harmonic phonon–phonon interaction, as reported in [39]. The weak broad band located at 520–580 cm^{-1} is due to overlap of several peaks located in this region. In fact Souissi et al. [38] have reported the presence of five peaks at 538, 556, 579, 585 and 590 cm^{-1}: in particular the bands at 556 and 585 cm^{-1} are attributed to the presence of impurities and structural defects (oxygen vacancies and Zn interstitials) in the deposits [40].

Once ascertained that deposition at 60 °C gives more uniform and compact films, we concentrated on the effect of zinc nitrate concentration in solution and of the applied

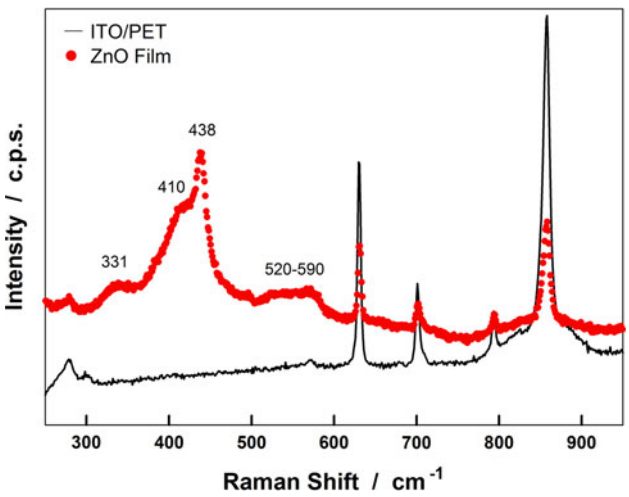

Fig. 3 Raman spectrum of a ZnO film deposited at −1.4 V(MSE) and 60 °C from a 0.05 M $Zn(NO_3)_2{\cdot}6H_2O$ solution. For comparison, a spectrum of the ITO/PET substrate is also shown

potential. Figure 4 shows deposition curves from electrolytes containing different amounts of nitrate salt: shape of the curves is similar, but deposition c.d. increases with increasing nitrate content in the electrolyte. Interestingly, reagent concentration affects both morphology and crystalline structure of deposited layers: comparison between diffraction patterns of Fig. 5 reveals that films deposited from more concentrated solutions show a polycrystalline structure and a lower crystalline degree, whilst for more diluted electrolytes film tends to grow according to preferential orientations, becoming almost monocrystalline at the lowest concentration. This also results in a different morphology, as shown by SEM pictures of Fig. 6: high magnification pictures (left part) reveal that morphology changes from a pyramidal compact one, for the 0.05 M nitrate solution, to a less dense petal-like aspect, for an intermediate nitrate concentration; for the most diluted solution (0.01 M $Zn(NO_3)_2{\cdot}6H_2O$) film morphology changes drastically, being film composed by nearly hexagonal nanorods oriented perpendicular to the substrate, as already reported [19–21]. Also compactness of ZnO films is influenced by nitrate concentration, as suggested by the low magnification pictures in the right part of the same figure: with decreasing zinc nitrate concentration covering of the substrate is not complete due to the presence of voids. This fact was confirmed by EDS analysis performed on the sample, showing higher peak relative to In (present in the substrate) for films deposited from more diluted solutions. We mention that also films deposited from a 0.1 M $Zn(NO_3)_2{\cdot}6H_2O$ solution showed the presence of voids, so we conclude that the most compact layer is obtained from the solution with 0.05 M of zinc nitrate.

Similarly, also the applied potential affects the characteristics of deposited ZnO films. This influence was investigated comparing results of potentiostatic depositions carried out at 60 °C from the same solution (0.05 M $Zn(NO_3)_2{\cdot}6H_2O$). Changing electrode potential from −1.4 to −1.3 V(MSE) shape of deposition curve remains similar to that reported in Fig. 1, but cathodic c.d. decreases sensibly (Fig. S2 in ESM): a nearly constant value of about −0.12 mA cm^{-2} was recorded after the transient. At −1.2 V(MSE) deposition current was very low (∼−0.05 mA cm^{-2}). Once again, crystalline degree of the films changes: only few small and broad XRD peaks are present for the film deposited at −1.3 V, whilst ZnO deposited at −1.2 V displays a disordered structure (Fig. S3 in ESM). Moreover, with increasing deposition potential morphology changes, with partial coverage of the substrate by the oxide consisting of smaller crystallites and this indicates that oxide nucleation is reduced to limited areas of the substrate. Values of crystallite size, estimated using Schrerrer's formula [34] for oxides deposited under different conditions, are reported in Table 1.

3.2 Cl-doped ZnO and thermal treatment

Doping ZnO with chlorine is reported to improve carrier concentration whilst maintaining a good mobility and optical transparency of the films [28, 29]. Hence we have deposited Cl-doped films, also to compare their characteristics with the other films. For this aim, we used the same conditions as before (potentiostatic deposition at −1.4 V/MSE and 60 °C from a 0.05 M nitrate aqueous solution), simply adding to the electrolyte small concentrations (1–10 mM) of $ZnCl_2$.

Deposition curves maintain a shape similar to that in Fig. 1, only with a reduced circulating current (an almost constant value of −0.2 mA cm^{-2} is attained for a chloride concentration of 5 mM), which can be attributed to a complexing action of chloride ions towards zinc ones. EDS analysis confirms incorporation of Cl into deposited films

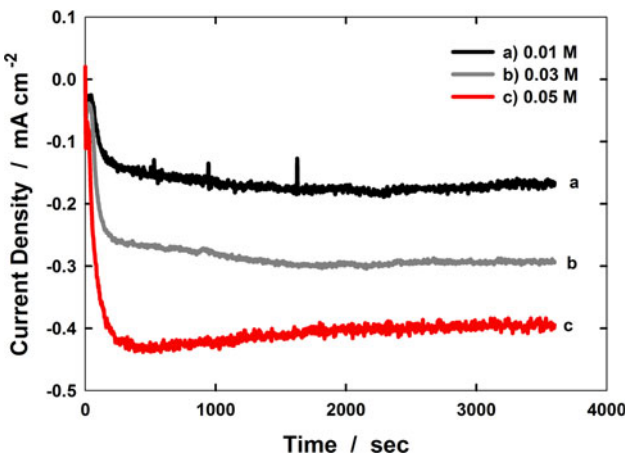

Fig. 4 Current density versus time during potentiostatic deposition of ZnO films at −1.4 V(MSE) and 60 °C from $Zn(NO_3)_2{\cdot}6H_2O$ solutions with different concentration: *a* 0.01 M; *b* 0.03 M; *c* 0.05 M

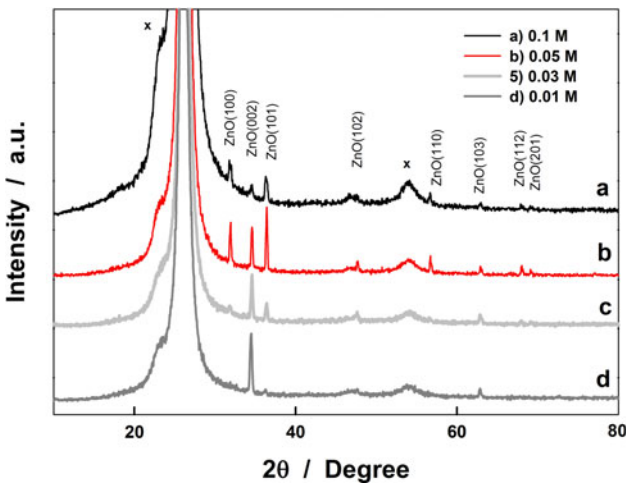

Fig. 5 XRD diffraction patterns for the ZnO films of Fig. 4. *Peaks* marked with *x* are relative to the ITO/PET substrate

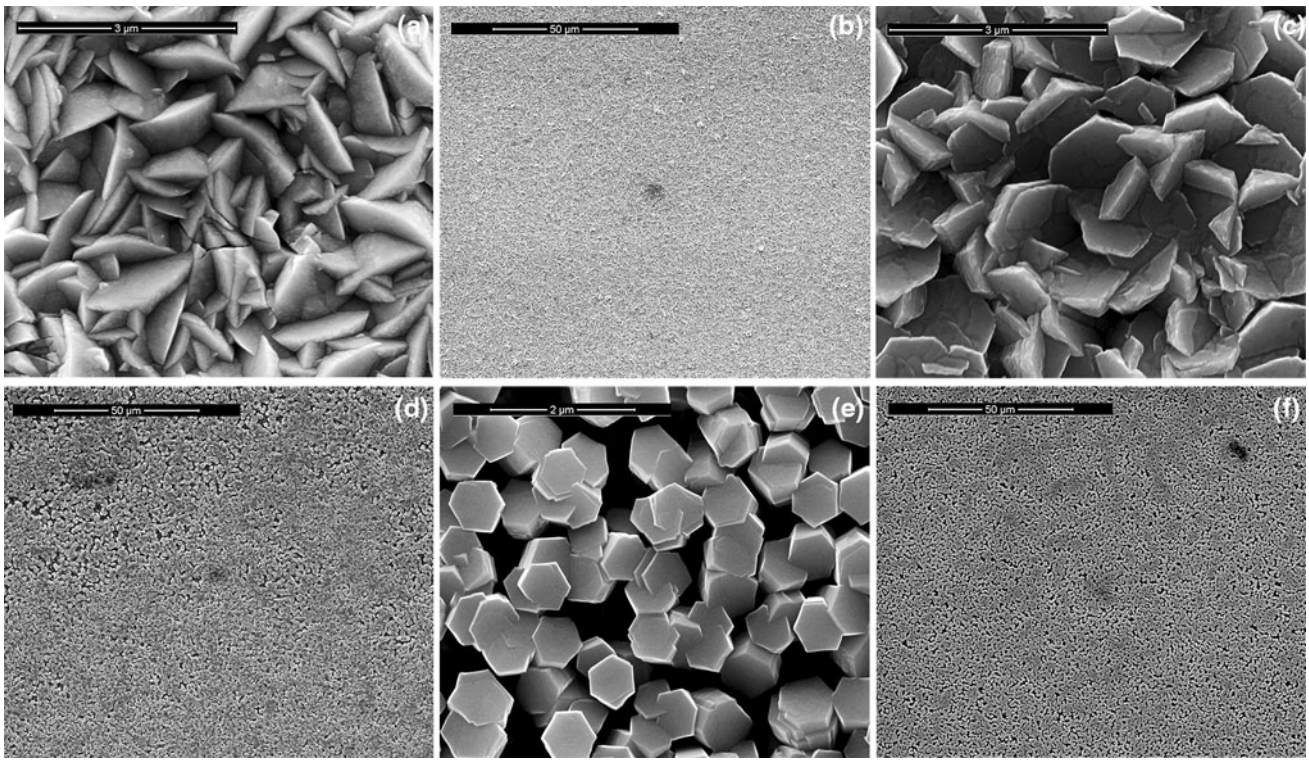

Fig. 6 FEG-ESEM images of ZnO films deposited at −1.4 V(MSE) and 60 °C from $Zn(NO_3)_2{\cdot}6H_2O$ solutions with different concentration: **a** and **b** 0.05 M; **c** and **d** 0.03 M; **e** and **f** 0.01 M

Table 1 Mean crystallite size of ZnO deposits calculated applying the Schrerrer's equation

Temperature (°C)	Nitrate conc. (mol/l)	Dep. potential (V/MSE)	*D* (nm)
40	0.05	−1.4	15
60	0.05	−1.4	33
60	0.03	−1.4	23
60	0.01	−1.4	25
60	0.05	−1.3	23
60	0.05	−1.2	–

(Fig. 7a), with an increasing quantity for increasing concentration in solution, as shown in Fig. 7b; it is worth to mention that Cl concentration reported in the figure was homogeneous in different parts of the films for all concentrations except the highest one, where a dispersion of values comprised within the error bar was measured in different points. Cl incorporation into the film occurs through formation of $ZnCl^+$ complexes in solution, followed by their reaction at the electrode [41]:

$$ZnCl^+ + 2OH^- \Rightarrow ZnO \downarrow + H_2O + Cl^- \quad (3)$$

Reaction (3) leads to ZnO film growth and to the release of most chloride ions in solution; however, some of them remain trapped into the film, forming a shallow donor level within the oxide band gap [29, 42]. No major changes in film crystallinity follow Cl incorporation: films remain polycrystalline in structure (see dispersion of Fig. 2), with only an increased importance of the (002) peak and an almost equal crystallite size (about 30 nm). As for morphology, film was compact and consists of irregular microstructures, whose dimension is smaller for higher Cl concentrations (Fig. S4 in ESM).

In order to study the effect of annealing on ZnO films (with or without Cl), depositions were performed on ITO/Glass substrates. For avoiding any influence on ZnO electrodeposition, we used a film of ITO having the same characteristics (thickness and surface resistivity) of the ITO on PET employed in the experiments already shown. In fact, no changes in growth curves, crystallinity and morphology of deposits were observed.

Thermal treatment of all deposited films was carried out in air at 150 °C for 2 or 5 h [43]. Sometimes also a treatment at 350 °C for 2 h was carried out. No relevant changes were observed neither in films morphology, which remains similar to that shown in Fig. 6a, b (Fig. S5 in ESM), nor in their XRD dispersion, with an average grain size always close to 30 nm (Fig. S6 in ESM). This means a slight grain enlargement only for films deposited from diluted solutions or at 40 °C (see Table 1), whilst films deposited from a 0.05 M nitrate solution at 60 °C do not

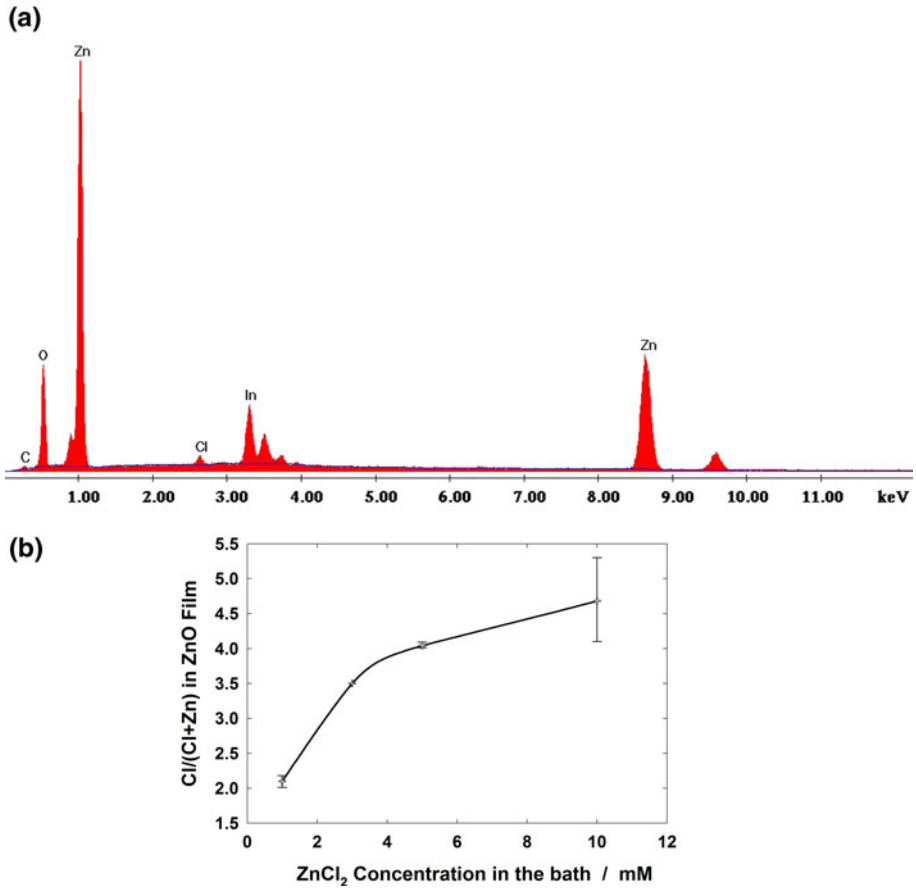

Fig. 7 **a** EDS spectrum of a ZnO film deposited at −1.4 V(MSE) and 60 °C from a bath containing 0.05 M of $Zn(NO_3)_2{\cdot}6H_2O$ and 5 mM of $ZnCl_2$. **b** Cl/(Cl + Zn) atomic ratio into the ZnO:Cl deposit versus concentration of $ZnCl_2$ in the electrodeposition bath

change their grain size. Also relative intensity of XRD peaks for films incorporating Cl is not affected by these thermal treatments. On the contrary, in the next section we will see that thermal treatment influences the behaviour of the films under illumination.

3.3 Photoelectrochemical study

The photoelectrochemical behaviour of the different films, before and after thermal treatment, was investigated in aerated quasi-neutral 0.1 M Na_2SO_4 solution (pH 5.7). For each sample, first the photocurrent response was measured at its open circuit potential (U_{oc}) and the photocurrent spectrum was recorded. Then, the dependence of the photocurrent on electrode potential was investigated under illumination with different wavelengths. Because all samples showed anodic photocurrent, according to the reported n-type nature of ZnO films [8], the investigated range of potential was normally positive with respect to U_{oc}.

Figure 8 shows two photocurrent action spectra (corrected for the photon emission of the lamp-monochromator system, see Sect. 2) for the ZnO film of Fig. 6a, b: apart from the photocurrent intensity, spectra, recorded at U_{oc} and $U_e = U_{oc} + 0.1$ V, display the same shape, with a slight shoulder at around 330 nm. In fact, the same value of optical gap (3.48 eV) was derived from both spectra assuming direct optical transitions, and thus processing data of Fig. 8 according to the formula [44]:

$$(i_{ph}hv)^2 \propto (hv - E_g) \quad (4)$$

where i_{ph} is the corrected photocurrent, hv the photon energy and E_g the optical gap of the film.

The increase of photocurrent intensity at less negative potentials follows a larger potential drop within the space-charge region in an n-type material. This is confirmed both by the current transients recorded chopping manually the light under monochromatic irradiation (Fig. 9) and by the photocurrent versus potential curves (Fig. 10). The first experiments display an anodic stationary photocurrent with the presence of spikes of the same sign, whilst photocharacteristics have a complex shape, with an initial rise of the photocurrent followed by a maximum and a plateau for very high biases; also a remarkable hysteresis of these curves between forward and back scan and between successive scans suggests some modification under illumination when going towards positive potentials. Very similar results were observed in the photoelectrochemical behaviour of Cl-doped films as for both the anodic photocurrent intensity and the shape of the photocurrent versus potential curves.

Some relevant changes in the behaviour under illumination were observed after performing thermal treatments on the films; the most important one is reported in Fig. 11, which compares the photocurrent spectra of the same film before and after thermal treatments. Two main changes are evident: (a) a step increase in photocurrent intensity; (b) a change of shape in the long wavelength region, with a more evident shoulder (almost a plateau) at around 330 nm. This second aspect is also reflected in a slight decrease of the optical gap values after thermal treatment of the films, as reported in Table 2, with values approaching 3.2 eV. This last is the reported band gap for crystalline ZnO [8]. Thus, after annealing in air, behaviour of film under illumination conforms more to that of crystalline zinc oxide, as confirmed also by the photocurrent versus potential curve of Fig. 12, showing more regular shape and almost no hysteresis. Comparison between photocharacteristics recorded at different wavelengths for the different films reveals also a sensible anodic shift (300–400 mV) in the photocurrent onset potential (U_{fb}, estimated as the point where photocurrent begins to rise steeply) after thermal treatment (see Table 2). This means that the photocurrent increase of Fig. 11 occurs in the presence of lower potential drops into the semiconductor space-charge region, as detailed in Table 2. This last finding can be attributed to a higher crystallinity degree of the ZnO layer due to the more severe conditions of annealing. This explanation is further supported by the progressive decrease of the band gap values with the annealing conditions also showed in Table 2, indicating a progressive decrease of defect concentration in the layer. In reading last column of Table 2, it must be mentioned that for the TT2 sample, U_{oc} was −0.51 V/MSE, whilst as prepared and TT1 samples have U_{oc} values of −0.62 and −0.61 V/MSE, respectively.

The photoelectrochemical study suggests that as-deposited ZnO films consist of nanocrystalline grains embedded in an amorphous oxide matrix: the optical gap values measured, higher than that reported for the crystalline phase, derive

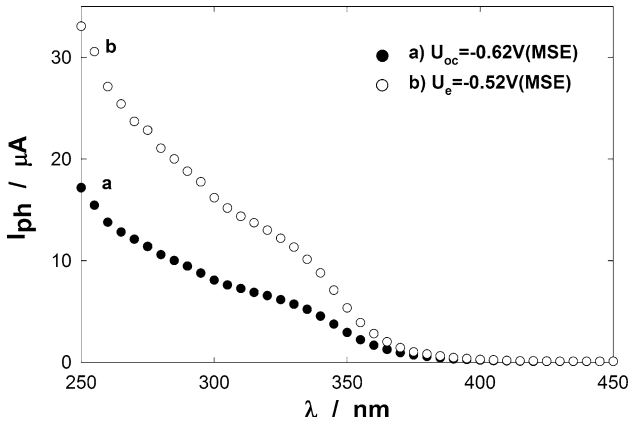

Fig. 8 Photocurrent spectra, recorded at different electrode potentials, for a ZnO film deposited at −1.4 V(MSE) and 60 °C from a 0.05 M $Zn(NO_3)_2{\cdot}6H_2O$ solution. *a* $U_e = U_{oc} = -0.62$ V(MSE); *b* $U_e = -0.52$ V(MSE)

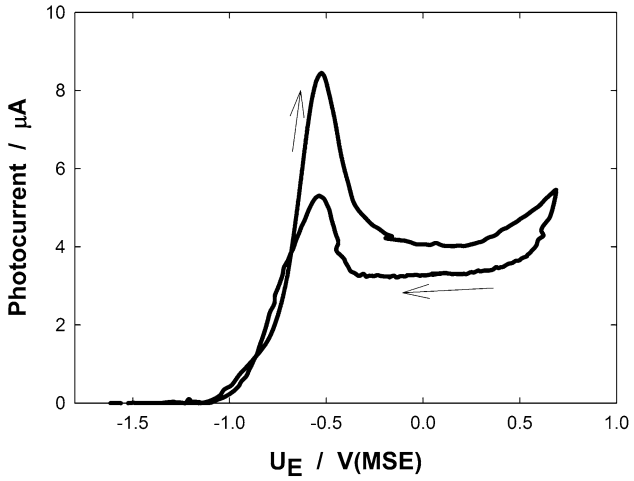

Fig. 10 Photocurrent versus electrode potential at λ = 330 nm for the ZnO film of Fig. 8

Fig. 9 Photocurrent transients under monochromatic irradiation with λ = 330 nm for the ZnO film of Fig. 8.
a $U_e = U_{oc} = -0.62$ V(MSE);
b $U_e = -0.52$ V(MSE)

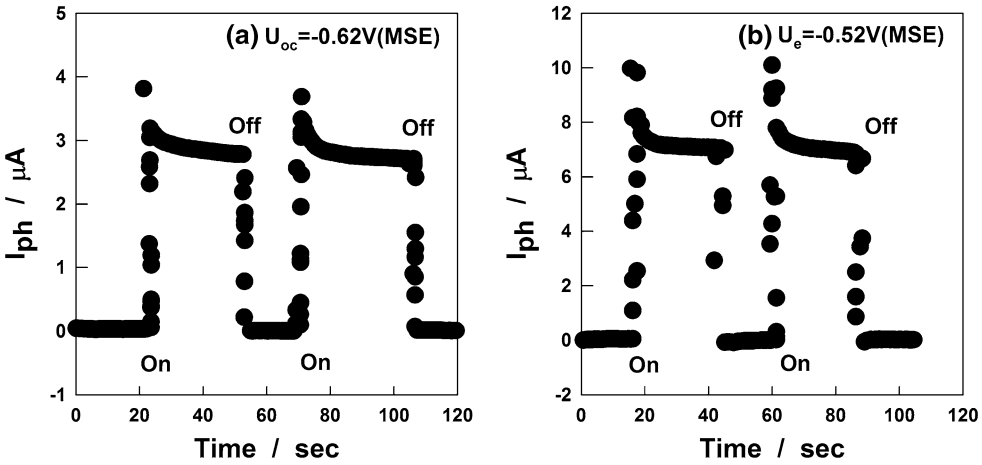

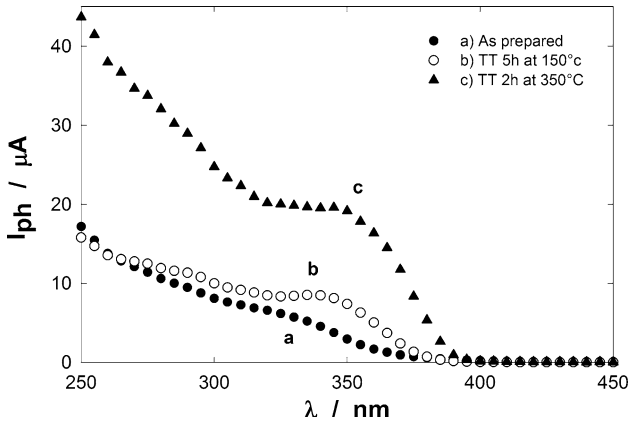

Fig. 11 Photocurrent spectra of ZnO films deposited at −1.4 V(MSE) and 60 °C from a 0.05 M $Zn(NO_3)_2{\cdot}6H_2O$ solution, before and after different thermal treatments: *a* as-prepared; *b* annealed at 150 °C for 5 h; *c* annealed at 350 °C for 2 h

Table 2 Optical gap and flat band potential (U_{fb}) of ZnO films before and after thermal treatments (TT)

Sample	E_g (eV)	i_{ph} onset (V/MSE)	U_{oc}–U_{fb} (V)
ZnO	3.48	−1.01 ± 0.04	0.39 ± 0.04
ZnO + TT1	3.36	−0.68 ± 0.03	0.07 ± 0.03
ZnO + TT2	3.24	−0.71 ± 0.04	0.20 ± 0.04
ZnO:Cl	3.52	–	–
ZnO:Cl + TT1	3.23	–	–

The value of U_{fb} was estimated from photocurrent onset in the photocurrent versus potential curves. (*TT1* 150 °C for 5 h; *TT2* 350 °C for 2 h)

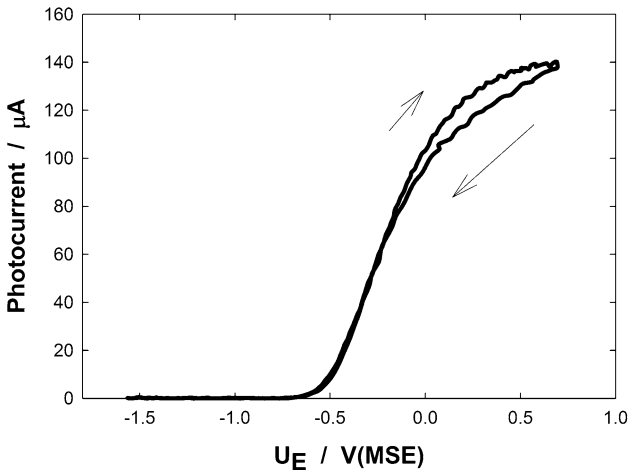

Fig. 12 Photocurrent versus electrode potential at λ = 330 nm for a ZnO film deposited at −1.4 V(MSE) and 60 °C from a 0.05 M of $Zn(NO_3)_2{\cdot}6H_2O$ solution, and annealed at 150 °C for 5 h in air

from the response under illumination of localized electronic states originated from these disordered regions [18, 45, 46]. Thermal treatment, although not influencing appreciably grain size of the crystallites, reduces the disordered regions and likely produces an annealing of defects and irregularities within the oxide film. This produces reduction of traps and finally a more efficient transport of the photogenerated carriers within the oxide film, with a consequent rise of photocurrent intensity.

4 Conclusions

Structure and morphology of ZnO films electrodeposited from zinc nitrate aqueous solutions depend on the experimental parameters (temperature, electrode potential, concentration of nitrate in solution). More uniform and compact films, with larger grain size, were obtained by electrodeposition at −1.4 V(MSE) and 60 °C from a 0.05 M $Zn(NO_3)_2{\cdot}6H_2O$ solution. Adding zinc chloride to the electrolyte resulted in Cl species incorporation into the oxide film with a larger concentration for higher chloride ion content in the starting solution.

Deposited films were generally polycrystalline in structure, even if growth according to preferential planes occurs in certain conditions. The average grain size, slightly varying with the experimental parameters, is in the order of few tenths of nanometres.

Thermal treatments, performed in air for different times at 150 or 350 °C, do not induce major changes in morphology or in the crystalline structure of the films, whilst they affect noticeably their behaviour under illumination.

The photoelectrochemical investigation of the films reveals the n-type semiconducting nature of all samples investigated, and suggests that as-deposited films consist of nano-crystallites embedded in a disordered matrix: this lowers the intensity of photoresponse whilst giving higher values of optical gap. After thermal treatment, the measured gap decreases towards the value reported for the crystalline oxide, and the photocurrent intensity rises sensibly, indicating a reduction of defects and traps originated from the disordered regions of the oxide.

No apparent benefits in the semiconducting properties of the films were observed after incorporation of Cl species into the films.

Acknowledgments This study was partially funded by the European Community through the Programma Operativo Nazionale Ricerca e Competitività 2007–2013 (PON01_01725 Project).

References

1. Poortmans J, Arkhipov V (2006) Thin film solar cells: fabrication, characterization and application. Wiley, Chichester
2. Singh UP, Patra SP (2010) Progress in polycrystalline thin-film $Cu(In,Ga)Se_2$ solar cells. Int J Photoenergy doi:10.1155/2010/468147

3. Basol P (2010) Commercialization of commercialization of high efficiency low cost CIGS Technology based on electroplating: final technical progress report (NAR-7-77015-10). National Renewable Energy Laboratory, Lakewood
4. Saji VS, Cjoi SS, Lee C-W (2011) Progress in electrodeposited absorber layer for $CuIn_{(1-x)}Ga_xSe_2$ (CIGS) solar cells. Sol Energy 85:2666–2678
5. Inguanta R, Livreri P, Piazza S, Sunseri C (2010) Fabrication and photoelectrochemical behavior of ordered CIGS nanowire arrays for application in solar Cells. Electrochem Solid State Lett 13:K22–K25
6. Gordon RG (2000) Criteria for choosing transparent conductors. MRS Bull 2000:52–57
7. Ingram BJ, Gonzalez GB, Kammler DR, Bertoni MI, Mason TO (2004) Chemical and structural factors governing transparent conductivity in oxide. J Electroceramics 13:167–175
8. Pearton SJ, Norton DP, Ip K, Heo YW, Steiner T (2005) Recent progress in processing and properties of ZnO. Prog Mater Sci 50:293–340
9. Singh A, Kumar A, Suri N, Kumar S, Kumar M, Khanna PK, Kumar D (2009) Structural and optical characterization of ZnO thin films deposited by sol–gel. J Optoelctron Adv Mater 11:790–793
10. Lupan O, Shishiyanu S, Chow L, Shishiyanu T (2008) Nanostructured zinc oxide gas sensors by successive ionic layer adsorption and reaction method and rapid photothermal processing. This Solid Films 516:3338–3345
11. Prajapati CS, Sahay PP (2012) Effect of precursors on structure, optical and electrical properties of chemically deposited nanocrystalline ZnO thin films. Appl Surf Sci 258:2823–2828
12. Tarwal NL, Shinde VV, Kamble AS, Jadhav PR, Patil DS, Patil VB, Patil PS (2011) Photoluminescence and photoelectrochemical properties of nanocrystalline ZnO thin films synthesized by spray pyrolysis technique. Appl Surf Sci 257:107889–110794
13. Zhang P, Wei H, Cong G, Hu W, Fan H, Wu J, Zhu Q, Liu X (2008) Effects of disk rotation rate on the growth of ZnO films by low-pressure metal–organic chemical vapor deposition. Thin Solid Films 516:925–928
14. Hupkes J, Rech B, Calnan S, Kluth O, Zastrow U, Siekmann H, Wutting M (2006) Material study on reactively sputtered zinc oxide for thin film silicon solar cells. Thin Solid Films 502:286–291
15. Yan C, Xue D (2007) Electroless deposition of aligned ZnO tapertubes in a strong acidic medium. Electrochem Commun 9:1247–1251
16. Matei E, Enculescu I (2011) Electrodeposited ZnO fils with high UV emission properties. Mater Res Bull 46:2147–2154
17. Dalchiele EA, Giorgi P, Marotti RE, Martin F, Ramos-Barrado JR, Ayouci R, Leinin D (2001) Electrodeposition of ZnO thin films on *n*-Si(100). Sol Energy Mater Sol Cells 70:245–254
18. Marotti RE, Giorgi P, Machado G, Dalchiele EA (2006) Crystallite size dependance of band gap Energy for electrodeposited ZnO grown at different temperatures. Sol Energy Mater Sol Cells 90:2356–2361
19. Lupan O, Pauporte T, Chow L, Viana B, Pelle F, Ono LK, Roldan Cuenya B, Heinrich H (2010) Effects of annealing on properties of ZnO thin films prepared by electrochemical deposition in chloride medium. Appl Surf Sci 256:1895–1907
20. Liu R, Vertegel AA, Bohannam EW, Sorenson TA, Switzer JA (2001) Epitaxial electrodeposition of zinc oxide nanopillars on single-crystal gold. Chem Mater 13:508–512
21. Pauporte T, Cortes R, Froment M, Beaumont B, Lincot D (2002) Electrocrystallization of epitaxial zinc oxide onto gallium nitride. Chem Mater 14:4702–4708
22. Belghiti HEI, Pauporte T, Lincot D (2008) Mechanistic study of ZnO nanorod array electrodeposition. Phys Stat Sol A 205:2360–2364
23. Yang J, Lin Y, Meng Y, Liu Y (2012) A two-step route to synthesize highly oriented ZnO nano tube arrays. Ceram Int. doi: 10.1016/j.ceramint.2012.02.033
24. Kohan AF, Ceder G, Morgan D, Van de Walle CG (2000) First-principles study of native point defect in ZnO. Phys Rev B 61: 15019–15027
25. Islam MM, Ishizuka S, Yamada A, Matsubara K, Niki S, Sakurai T, Akimoto K (2011) Thickness study of Al:ZnO film for application as a window layer in $Cu(In_{1-x}Ga_x)Se_2$ thin film solar cell. Appl Surf Sci 257:4026–4030
26. Mei YF, Fu RKY, Siu GG, Wong KW, Chu PK, Wang RS, Ong HC (2006) Nitrogen binding behaviour in ZnO films with time-resolved cathodoluminescence. Appl Surf Sci 252:8131–8134
27. Steinhauser J, Fay S, Oliveira N, Vallant-Sauvain E, Zimin D, Kroll U, Ballif C (2008) Electrical transport in boron-doped polycrystalline zinc oxide thin films. Phys Stat Sol A 205:1983–1987
28. Tchelidze T, Chikoidze E, Gorochov O, Galtier P (2007) Perspectives of chlorine doping of ZnO. Thin Solid Films 515: 8744–8747
29. Rousset J, Saucedo E, Herz K, Lincot D (2011) High efficiency CIGS based solar cells with electrodeposited ZnO:Cl as transparent conducting oxide front contact. Prog Photovoltaics Res Appl 19:537–546
30. Besbes S, Ben Ouada H, Davenas J, PonsonnetL L, Jaffrezic N, Alcouffe P (2006) Effect of surface treatment and functionalization on the ITO properties for OLEDs. Mater Sci Eng C 26: 505–510
31. International Centre for Diffraction Data (2007) Card # 36-1451. Zinc oxide/zincite
32. Yoshida T, Komatsu D, Shimokawa N, Minoura H (2004) Mechanism of cathodic electrodeposition of zinc oxide thin films from aqueous zinc nitrate bath. Thin Solid Films 451–452:166–169
33. Nobial M, Devos O, Mattos OR, Tribollet B (2007) The nitrate reduction process: a way for increasing interfacial pH. J Electroanal Chem 600:87–94
34. West AR (1985) Solid state chemistry and its applications. Wiley, Chichester, p 173
35. Calleja JM, Cardona M (1977) Resonant Raman scattering in ZnO. Phys Rev 16:3753–3761
36. Damen TC, Porto SPS, Tell B (1966) Raman effect in zinc oxide. Phys Rev 142:570–574
37. Souissi A, Sartel C, Sayari A, Meftah A, Lusson A, Galtier P, Sallet V, Oueslati M (2012) Zn- and O-polar surface effects on Raman mode activation in homoepitaxial ZnO thin films. Solid State Commun 152:794–797
38. Souissi A, Sartel C, Amiri G, Meftah A, Lusson A, Galtier P, Sallet V, Oueslati M (2012) Raman study of activated quasi-modes due to misorientation of ZnO nanowires. Solid State Commun. doi:10.1016/j.ssc.2012.06.004
39. Cusco R, Llado EA, Ibanez J, Artus L, Jimenez J, Wang B (2007) Temperature dependence of Raman scattering in ZnO. Phys Rev B 75:165202
40. Wahab R, Ansari SG, Kim YS, Seo HK, Kim GS, Khang G, Shin H-S (2007) Low temperature solution synthesis and characterization of ZnO nano-flowers. Mater Res Bull 42:1640–1648
41. Goux A, Pauporte T, Chivot J, Lincot D (2005) Temperature effects on ZnO electrodeposition. ElettrochimActa 50:2239–2248
42. Rousset J, Saucedo E, Lincot D (2009) Extrinsic doping of electrodeposited zinc oxide films by chlorine for transparent conducting oxide application. Chem Mater 19:534–540
43. Lupan O, Pauporte T, Tiginyanu IM, Ursaki VV, Sontea V, Ono LK, Roldan Cuenya B, Chow L (2011) Comparative study of hydrothermal treatment and thermal annealing effects on the properties of electrodeposited micro-columnar thin films. Thin Solid Films 519:7738–7749
44. Taner A, Kul M, Turan E, Senol Aybek A, Zor M, Taskopru T (2011) Optical and structural properties of zinc oxide films with different thicknesses prepared by successive ionic layer adsorption and reaction method. This Solid Films 520:1358–1362

45. Tan ST, Chen BJ, Sun XW, Fan WJ, Knok HS, Zhang XH, Chua SJ (2005) Blueshift of optical band gap in ZnO thin films grown by metal–organic chemical-vapor deposition. J Appl Phys 98:013505

46. Mott NF, Davis EA (1979) Electronic processes in non-crystalline materials. Oxford University Press, Oxford